Research Square

Preprints are preliminary reports that have not undergone peer review.
They should not be considered conclusive, used to inform clinical practice,
or referenced by the media as validated information.

Torque ripple suppression in switched reluctance motors using iterative learning control to optimize the torque sharing function

Jingbo Wu

wubocn2005@163.com

Henan University of Science and Technology

Shaofeng Li

Henan University of Science and Technology

Yafeng Yang

Henan University of Science and Technology

Liuxi Li

Henan University of Science and Technology

Zhipeng Wang

Henan University of Science and Technology

Article

Keywords: Switched reluctance motor, Torque ripple suppression, Iterative learning control, Torque sharing function

Posted Date: November 2nd, 2026

DOI: https://doi.org/10.21203/rs.3.rs-11251026/v1

License: This work is licensed under a Creative Commons Attribution 4.0 International License.
Read Full License

Additional Declarations: No competing interests reported.

Torque ripple suppression in switched reluctance motors using iterative learning control to optimize the torque sharing function

Jingbo Wu*, Shaofeng Li [1], Yafeng Yang [1], Liuxi Li [1] & Zhipeng Wang [1]

[1]→College of Vehicle and Traffic Engineering, Henan University of Science and Technology, Luoyang, 471003, China; wubocn2005@163.com (Jingbo Wu*); 13839811672@163.com (Shaofeng Li [1]); 9906477@haust.edu.cn (Yafeng Yang [1]); 18439454706@163.com (Liuxi Li [1]); 17329449153@163.com (Zhipeng Wang [1]);

Abstract

Torque ripple caused by uneven torque transfer during phase commutation limits the low-speed steady-state performance of switched reluctance motors (SRMs). This paper proposes a control strategy that uses iterative learning control (ILC) to optimize the torque sharing function (TSF). Starting from a cosine TSF, the method uses the torque error recurring within each electrical cycle to update the TSF in the commutation region from one cycle to the next. The resulting reference torque distribution progressively approaches the actual electromagnetic torque response, thereby improving torque transfer between phases. An 8/6-pole SRM drive model is developed using ANSYS/Maxwell and MATLAB/Simulink to evaluate the proposed strategy. Compared with conventional TSF control, the proposed strategy reduces the torque ripple rate of the SRMs by 39.69%,38.86%, and 38.29% under low-speed steady-state operating conditions of 100 r/min, 200 r/min, and 400 r/min, respectively, demonstrating its effectiveness in suppressing torque ripple.

Keywords: Switched reluctance motor, Torque ripple suppression, Iterative learning control, Torque sharing function

1 Introduction

Switched reluctance motors (SRMs) offer a simple and robust structure, reliable operation, high energy conversion efficiency, and freedom from rare-earth materials, making them promising candidates for electric vehicle traction applications[1,2]. However, their doubly salient structure and pronounced magnetic saturation produce substantial torque ripple at low speeds, limiting their wider application in electric vehicles[3,4].

Control strategy optimization is a major approach to torque ripple suppression[5]. Among the available methods, torque sharing function (TSF) control has attracted considerable attention because of its simple structure and ease of implementation [6,7]. Ye et al.[8] and Li et al.[9] optimized the distribution of phase reference torques using TSFs to improve torque transfer during commutation. Fei et al.[10] proposed a modified TSF method that combines TSF profile optimization with closed-loop torque control to suppress torque ripple. Chen et al.[11] combined a cosine TSF with current compensation to reduce torque ripple at high speeds. Nevertheless, existing TSF strategies still rely on predefined function profiles and have limited adaptability to motor nonlinearities, leaving a mismatch between the actual and reference torques.

Iterative learning control (ILC) has received increasing attention as a means of improving SRM torque control accuracy because it uses errors from repeated operation to learn and apply corrections from cycle to cycle[12]. Lai et al.[13] used iterative learning to optimize the PWM duty cycle online at different rotor positions, improving current tracking under nonlinear operating conditions. Liu et al.[14] subsequently incorporated ILC into indirect torque control of SRMs, iteratively correcting the reference current using recurring torque errors to improve the torque-current mapping. Mahalakshmi et al. [15] compared the reference and actual torques and updated the phase current reference trajectories over successive iterations to optimize the current waveforms

and reduce torque ripple. Ren et al.[16] incorporated an iterative learning observer into deadbeat predictive current control to compensate for disturbances caused by parameter mismatch, thereby improving current control accuracy and robustness to parameter variations. The convergence, tracking performance, and robustness of PID-type [17] and PD-type [18] iterative learning algorithms have also been investigated, providing a theoretical basis for applying ILC to different control systems.

Building on these studies, this paper proposes an ILC-based TSF optimization strategy that combines a simple control structure with torque ripple suppression. For low-speed steady-state SRM operation, the method iteratively corrects the TSF using periodic torque errors, improving agreement between the reference and actual torques without substantially increasing control complexity. Simulation results indicate relatively fast convergence and a substantial reduction in torque ripple under the operating conditions considered.

2 Mathematical model of the SRM

The SRM has a doubly salient structure, with both the stator and rotor constructed from laminated silicon steel sheets, and exhibits pronounced nonlinear characteristics. Analysis of its mathematical model, together with finite-element modeling in Ansys, helps explain the mechanisms responsible for torque ripple and supports the development of more accurate control strategies.

SRM operation follows the principle of minimum reluctance [19], according to which magnetic flux tends to follow the path of least magnetic reluctance. The flux linkage ψ_j of phase j can be expressed as the product of the phase inductance $L_j\left(\theta,i_j\right)$ and winding current i_j. Thus, ψ_j is a function of current i_j and rotor position angle θ:

$$\psi_j\left(\theta,i_j\right)=L_j\left(\theta,i_j\right)i_j \tag{1}$$

Neglecting mutual inductance between phases, the voltage equation of the SRM is given by

$$\begin{aligned} U_j &= i_jR_j+\frac{d\psi_j}{dt} \\ &= i_jR_j+\frac{\partial\psi_j}{\partial i_j}\frac{di_j}{dt}+\frac{\partial\psi_j}{\partial\theta}\frac{d\theta}{dt} \end{aligned} \tag{2}$$

Where U_j is the terminal voltage of the phase-j winding and R_j is its resistance.

The mechanical dynamics are expressed as

$$T_j=J\frac{d\omega}{dt}+T_L+F\omega \tag{3}$$

where T_j is the electromagnetic torque of phase j, J is the moment of inertia, ω is the rotor angular velocity, T_L is the load torque, and F is the viscous damping coefficient.

Current i and electromagnetic torque T_e are related through the magnetic field energy W_f and magnetic co-energy W'. According to the principle of virtual displacement, the electromagnetic torque is obtained from the partial derivative of the magnetic co-energy with respect to rotor position angle:

$$T_e(i,\theta)=\frac{\partial W'(i,\theta)}{\partial\theta}=-\frac{\partial W_f(\psi,\theta)}{\partial\theta} \tag{4}$$

$$W'=\frac{1}{2}i\psi=\frac{1}{2}Li^2 \tag{5}$$

Substituting Eq. (5) into Eq. (4) yields

$$T_e=\frac{1}{2}i^2\frac{\partial L}{\partial\theta} \tag{6}$$

The nonlinear magnetic circuit of the SRM makes the relationships among flux linkage, inductance, current, and rotor position difficult to characterize, posing a substantial challenge to accurate modeling[20]. Finite-element simulations are therefore used to obtain the electromagnetic characteristics. Figure 1 shows the structure of a four-phase 8/6-pole SRM with clockwise rotor rotation. In the finite-element model, the initial position is defined by alignment of the rotor slot axis L1 with the stator winding axis A-A1. The rotor then rotates clockwise until the adjacent rotor slot axis L2 aligns with A-A1. This interval represents the electromagnetic interaction of one phase with a rotor pole over one cycle and corresponds to a mechanical rotation of 60°.

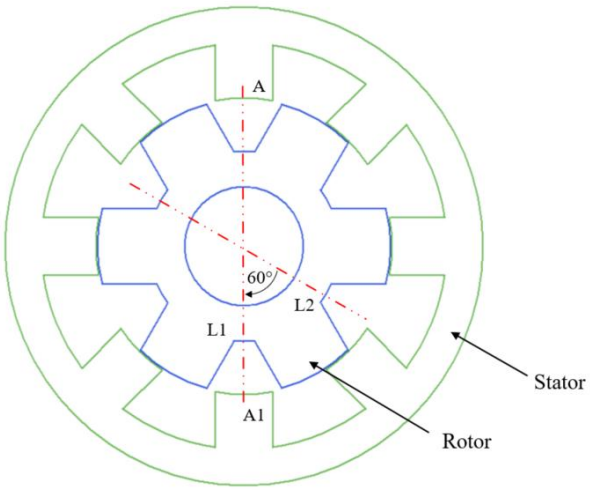


Fig. 1. Structure of the 8/6-pole SRM.

3 ILC-based TSF optimization

3.1 Torque sharing function

At low speeds, the SRM back electromotive force is relatively small, allowing the winding currents to track their commands effectively. The electromagnetic torque therefore closely reflects the distribution of phase currents, making coordinated phase torque allocation a suitable approach to low-speed torque ripple suppression. TSFs are widely used for this purpose because they provide an intuitive formulation, a clear physical interpretation, and straightforward integration with current control. For a specified total torque, a TSF distributes the torque among the phases according to a prescribed sharing law to generate the phase torque references. During commutation between adjacent phases, the current in one phase increases as that in the other decreases, maintaining a constant total torque and suppressing torque ripple. The phase sharing functions must sum to unity at every instant:

$$\begin{cases} \sum_{j=1}^{i} f_j(\theta) = 1 \\ 0 \le f_j(\theta) \le 1 \end{cases} \tag{7}$$

where i is the number of SRM phases and $f_j(\theta)$ is the sharing function of phase j.

Common TSF profiles include linear, cubic, cosine, and exponential functions. The reference torque $T_{ref}(j)$ assigned to each phase is related to the total reference torque T_{ref} by

$$T_{ref}(j) = T_{ref} \times f_j(\theta) \tag{8}$$

To enable the actual phase torques to track their TSF-based references accurately, the TSF should not vary excessively rapidly. A cosine TSF is therefore adopted in this study:

$$f_j(\theta) = \begin{cases} \frac{1}{2} - \frac{1}{2}\cos\frac{\pi}{\theta_{ov}}(\theta - \theta_{on}), \\ \theta_{on} \le \theta \le \theta_{on} + \theta_{ov}; \\ 1, \ \theta_{on} + \theta_{ov} \le \theta \le \theta_{off}; \\ \frac{1}{2} + \frac{1}{2}\cos\frac{\pi}{\theta_{ov}}\left(\theta - \theta_{off}\right), \\ \theta_{off} \le \theta \le \theta_{off} + \theta_{ov}; \\ 0, others. \end{cases} \tag{9}$$

where θ_{on}, θ_{ov}, and θ_{off} denote the turn-on angle, commutation overlap angle, and turn-off angle, respectively. The corresponding TSF profile is shown in Fig. 2.

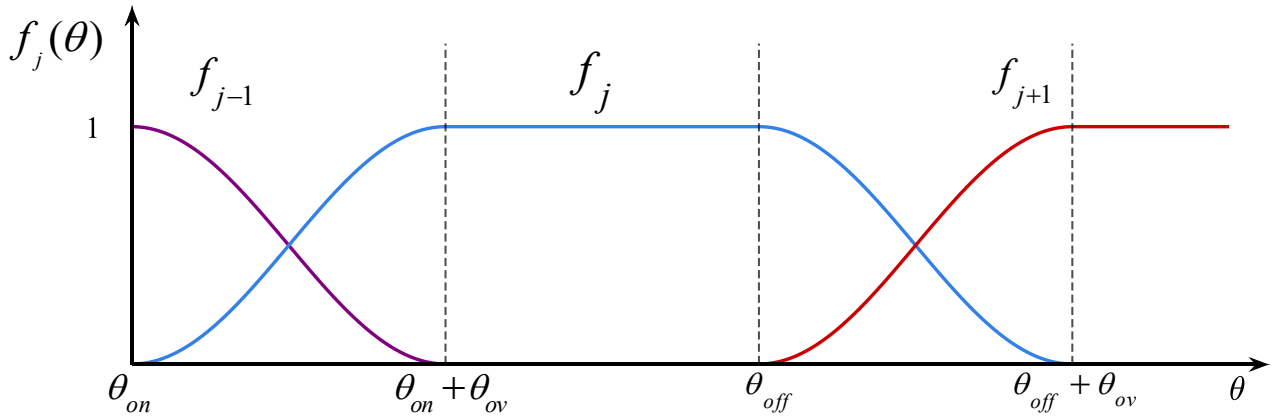


Fig. 2. Schematic of the cosine TSF.

As illustrated by the torque ripple mechanism in Fig. 3, when the k th phase rotor approaches the θ_{on} position of the incoming phase, the phase winding has just entered the conduction stage, and substantial alignment between the stator and rotor teeth has not yet been established. The phase inductance is therefore low, and its rate of change with rotor position is also relatively limited. According to the electromagnetic torque production mechanism of the SRM, rapid tracking of the reference torque at this stage requires the phase current to rise within a short interval. However, the available winding voltage, winding current dynamics, and operating capability of the power converter limit the rate of current rise. Consequently, the actual phase current cannot immediately reach the level required to produce the reference torque, causing the incoming-phase torque to lag behind its reference.

Similarly, as the k th phase rotor approaches the $\theta_{off}+\theta_{ov}$ position of the outgoing phase, its reference torque gradually decreases. However, residual current continues to flow in the winding and cannot decay rapidly enough to follow the reference torque reduction. This results in a discrepancy between the actual and reference torques of the outgoing phase. Thus, delayed torque buildup in the incoming phase and delayed torque decay in the outgoing phase coexist during commutation, preventing the actual phase torques from following the ideal torque transfer prescribed by the conventional TSF.

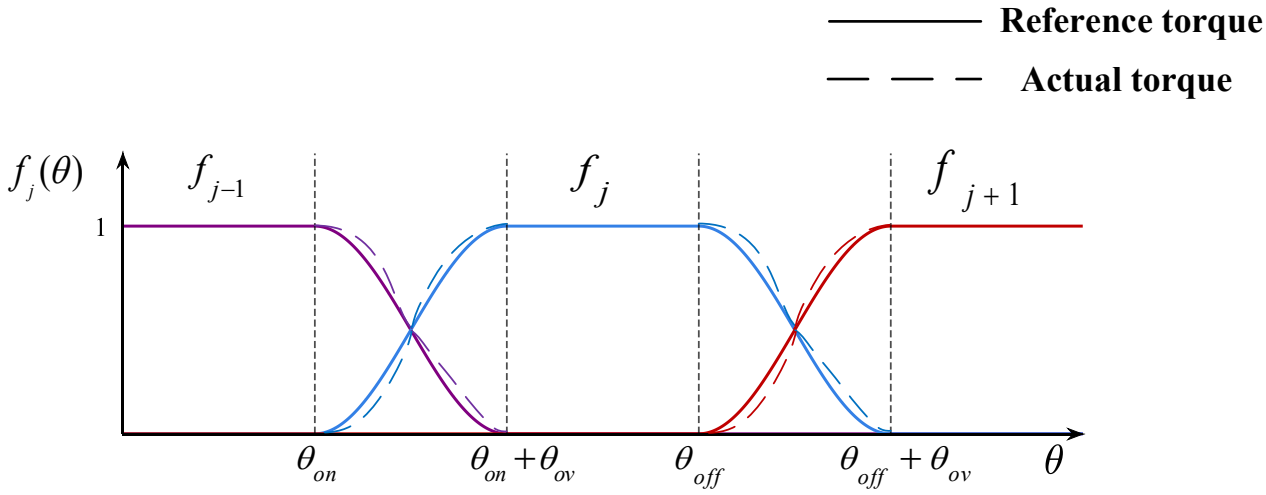


Fig. 3. Mechanism of torque ripple in TSF control.

The limitation of the conventional TSF therefore lies in the difficulty of consistently matching its prescribed torque distribution to the actual operating characteristics of the motor. Although it can reduce torque ripple, its ability to suppress periodic torque errors remains limited. A periodic learning strategy is therefore introduced into TSF control to learn and compensate for recurring errors online.

3.2 Iterative learning control

ILC is a control method for repetitive tasks. It updates the control input using errors recorded during the preceding cycle, progressively improving tracking performance over successive iterations. Since steady-state SRM operation is periodic, ILC is well suited to compensating for periodic torque errors.

Consider a control system operating over a prescribed time interval $t\in[0,T]$. At iteration k, the control input is $u_k(t)$, the actual output is $y_k(t)$, and the desired output is $y_d(t)$. The objective of ILC is to use the error $e_k(t)$ obtained at iteration k to update the input for iteration $k+1$, so that the output progressively approaches the desired trajectory. A typical learning law can be written recursively as

$$\begin{cases} u_{k+1}(t)=u_k(t)+L(e_k(t)) \\ e_k(t)=y_d(t)-y_k(t) \end{cases} \tag{10}$$

where $L(\cdot)$ is the learning operator that converts the previous iteration error into a control correction. For open-loop ILC, $L(\cdot)$ can be expressed as

$$L\left(e_k(t)\right)=G_p e_k(t)+G_I\int e_k(t)dt+G_D\frac{d}{dt}e_k(t) \tag{11}$$

The values of the learning coefficients G_p, G_I, and G_D, including whether individual coefficients are set to zero, determine whether the algorithm is of the P, PI, PD, D, or PID type.

Proportional-type ILC (P-ILC) is widely used because of its simple structure, ease of implementation, and practical applicability. It progressively compensates for repetitive errors by introducing a correction proportional to the previous iteration tracking error into the input update. Let $u_k(t)$ denote the control input at iteration k, $y_k(t)$ the system output, and $y_d(t)$ the desired output trajectory. The P-ILC update law is given by

$$\begin{cases} u_{k+1}(t) = u_k(t) + \lambda e_k(t) \\ e_k(t) = y_d(t) - y_k(t) \end{cases} \tag{12}$$

where λ is the learning gain, which governs the learning rate and influences system stability. The input for the next iteration consists of the current input and an error-based correction.

In practical SRM operation, magnetic saturation, parameter nonlinearities, and modeling errors prevent the torque output associated with a conventional TSF from matching the reference exactly. These deviations recur in the commutation region. Incorporating ILC into TSF optimization allows the reference torque to be corrected from cycle to cycle using periodic torque errors, consistent with the repetitive nature of low-speed steady-state SRM operation.

3.3 P-ILC-based TSF optimization

The proposed P-ILC-based optimization starts from a conventional cosine TSF and uses the actual torque error in each electrical cycle as the learning signal. The function values or local shape parameters are updated from cycle to cycle so that the resulting reference torque distribution better matches the electromagnetic response of the motor at the operating point. As learning proceeds, the torque distribution in the commutation region approaches an optimized trajectory for the operating conditions, reducing fluctuations in the total torque during commutation.

The standard discrete P-ILC law is expressed as

$$u_{k+1}(\theta) = u_k(\theta) + \lambda e_k(\theta) \tag{13}$$

where $u_k(\theta)$ is the control input at the discrete rotor position θ during iteration k, λ is the learning gain, and $e_k(\theta)$ is the corresponding error.

In this study, ILC is applied at the torque level to optimize the cosine TSF. The control input $u_k(\theta)$ in the preceding equation is therefore replaced by the TSF $f_k(\theta)$ at iteration k, giving

$$f_{k+1}(\theta) = f_k(\theta) + \lambda e_k(\theta) \tag{14}$$

where $f_k(\theta)$ is the TSF value at the discrete rotor position θ during iteration k, $e_k(\theta)$ is the torque error at that position, and λ is the learning gain. Figure 4 shows the ILC-TSF control architecture.

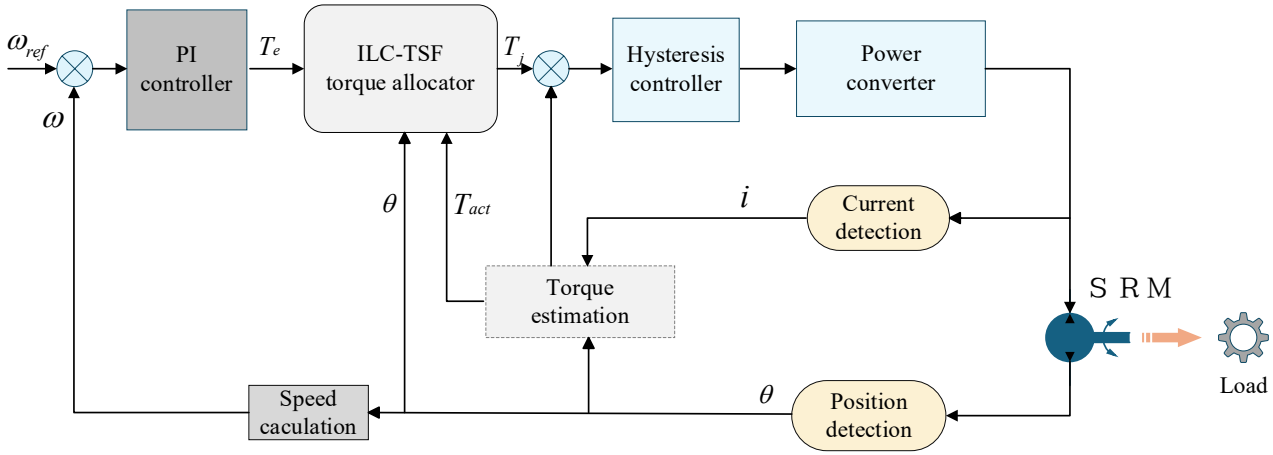


Fig. 4. Block diagram of the ILC-TSF control system.

The torque error is defined as the difference between the total reference torque and the actual output torque:

$$e_k(\theta) = T_e(\theta) - T_{act}(\theta) \tag{15}$$

Where $T_e(\theta)$ is the total reference torque and $T_{act}(\theta)$ is the actual torque at the discrete rotor position θ during iteration k. When the actual electromagnetic torque at a given position is below the reference, $e_k(\theta) > 0$, and the TSF value at that position is increased in the next cycle. Conversely, when the actual torque exceeds the reference, $e_k(\theta) < 0$, and the corresponding TSF value is decreased. This error-based adjustment uses the operating history to refine the sharing profile so that the reference torque allocation during commutation better matches the motor response. Figure 5 illustrates the construction of the TSF update law.

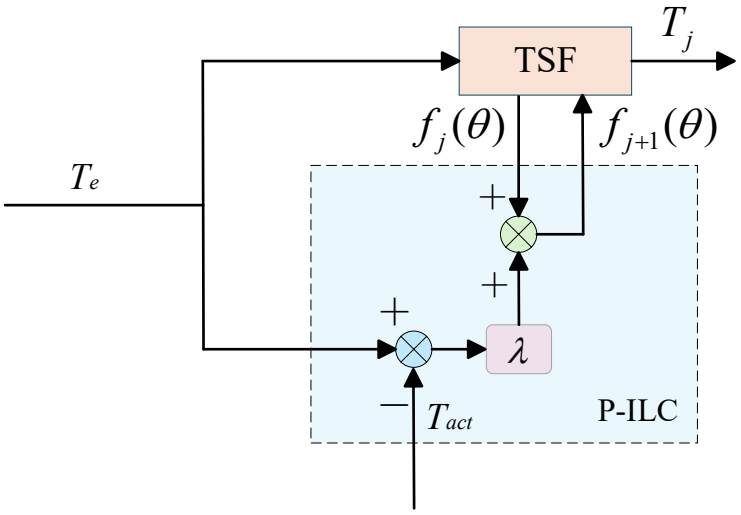


Fig. 5. Construction of the TSF update law.

The P-ILC update is applied primarily to the commutation region between adjacent phases. Let $f_k(\theta)$ denote the sharing function of the outgoing phase. Because the two sharing functions must sum to unity in this region, the sharing function of the incoming phase is $1 - f_k(\theta)$. Only one profile therefore needs to be updated iteratively; the other is obtained directly from the complement.

To satisfy the TSF constraints in Eq. (7), saturation is applied during the update. The resulting learning law is

$$f_{k+1}(\theta) = sat\left[f_k(\theta) + \lambda e_k(\theta)\right] \tag{16}$$

where $sat[\cdot]$ denotes the saturation function.

The conventional cosine TSF is used as the initial sharing function:

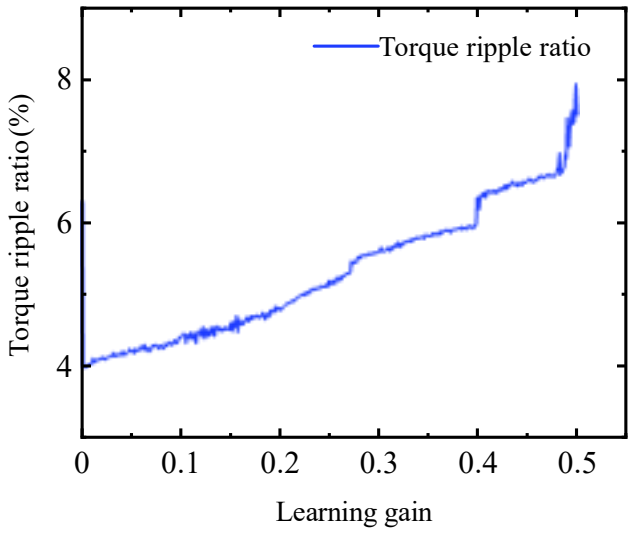
$$f_0(\theta) = f_{\cos}(\theta) \tag{17}$$

where $f_{\cos}(\theta)$ denotes the conventional cosine TSF. At the end of each operating cycle, the torque error recorded in that cycle is used to update the TSF-based reference torque for the next cycle. Repeated updates progressively reshape the conventional TSF toward a converged profile.

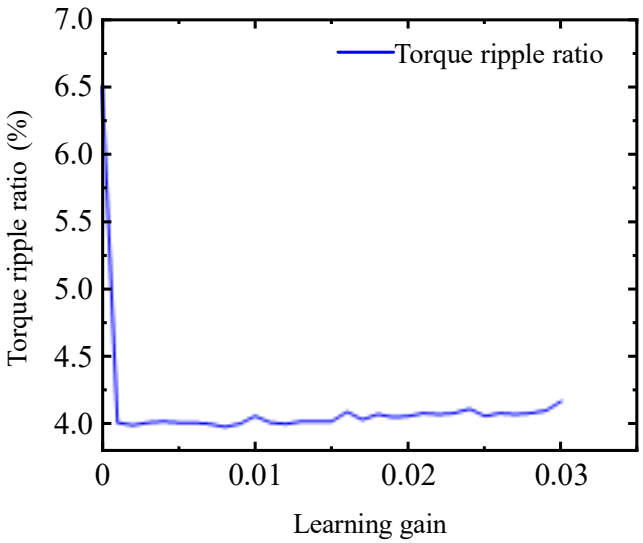
The learning gain determines the balance between stability and convergence speed. Different gains are therefore evaluated in simulation to identify the value that minimizes torque ripple while maintaining stable operation.

In this study, the operating condition of 200 r/min with a load torque of 10 N·m is selected as the baseline condition for tuning the learning gain. This speed lies between the other two test speeds of 100 r/min and 400 r/min, while the load torque is kept consistent with that used in the subsequent speed-comparison tests. Therefore, this operating point provides a unified reference for both learning-gain tuning and the subsequent validation of the proposed strategy at lower and higher speeds.

To ensure consistency in the comparison, all candidate learning gains are evaluated using the same initial cosine torque sharing function, identical initialization procedures, and the same torque-ripple evaluation method, while all other simulation settings are kept unchanged. The corresponding comparison results for different learning gains are presented in Fig. 6 and Table 1. It should be noted that the selected learning gain is an empirically tuned value determined under the baseline operating condition, and its effectiveness at other operating speeds is independently verified through the subsequent simulations.



(a) Overall variation curve



(b) Enlarged view of the local region

Fig. 6. Torque ripple ratio versus learning gain.

Table 1. Torque ripple ratio for selected learning gains in the low-gain range.

Learning gain λ	Torque ripple ratio	Remark
0	6.51%	Without ILC
0.003	4.01%	Low ripple
0.008	3.98%	Selected value
0.01	4.06%	Increased ripple
0.012	4.00%	Increased ripple
0.015	4.02%	Increased ripple

Figure 6(a) shows that the torque ripple ratio generally increases as the learning gain increases. As can be observed from the global curve in Fig. 6(a), the torque ripple rate initially decreases and then increases as the learning gain increases, indicating that an excessively large learning operator coefficient may lead to error overcompensation and consequently aggravate torque fluctuations in the system.

To identify an appropriate value in the low-gain range, Fig. 6(b) provides an enlarged view, while Table 1 summarizes representative results. Gains between 0.001 and 0.015 reduce torque ripple, although the degree of suppression varies. The lowest steady-state torque ripple ratio is obtained at $\lambda = 0.008$, indicating the best correction of periodic torque errors among the gains evaluated under these conditions. Accordingly, $\lambda = 0.008$ is used in the subsequent simulations.

The torque ripple ratio is used as the primary indicator for assessing convergence of the ILC-based TSF optimization. Let $T_{rip,k}$ denote the torque ripple ratio at iteration k. Its change between successive iterations is defined as

$$\Delta T_{rip,k} = \left| T_{rip,k} - T_{rip,k-1} \right| \tag{18}$$

When $\Delta T_{rip,k}$ falls below a prescribed threshold, further iterations provide little additional improvement

in torque ripple suppression, and the learning process is regarded as approximately converged. Considering the numerical precision of the simulations and the requirements of engineering analysis, a threshold of ε is adopted. Thus, when

$$\left|T_{rip,k} - T_{rip,k-1}\right| < 0.1\% \tag{19}$$

the system is considered approximately converged after iteration k.

Figure 7 shows the relationship between torque ripple ratio and iteration number at low speed.

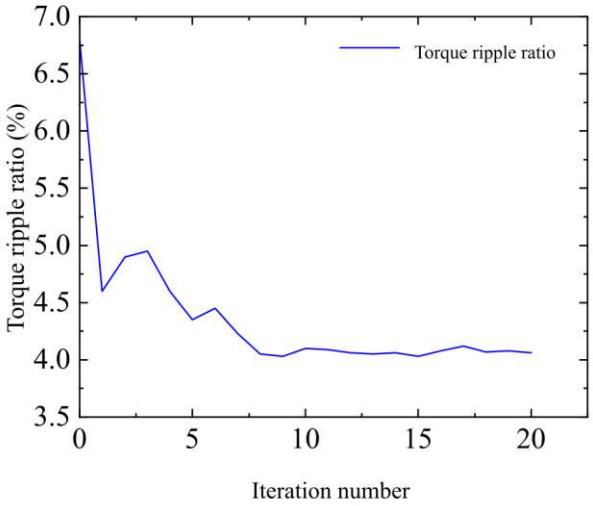


Fig. 7. Torque ripple ratio versus iteration number.

As can be observed from Fig. 7, the torque ripple rate exhibits an overall decreasing trend as the number of iterations increases, reaching its minimum at the 9th iteration. According to the statistical results and Eq. (19), the maximum change in the torque ripple rate between two successive iterations from the 9th to the 20th iteration is only 0.05 percentage points. With further iterations, the torque ripple rate does not decrease further but remains consistently stable at a relatively low level, indicating that the additional improvement achieved by subsequent iterations is limited. Therefore, the ILC is considered to have reached convergence at this stage, where the periodic torque error has been sufficiently suppressed.

In conclusion, the torque sharing function obtained at the 9th iteration is selected as the final optimized TSF. In the subsequent simulations, the iterative update is disabled, and the optimized function is directly employed for torque control. Since the optimized TSF is defined as a function of the rotor mechanical angle, it can be applied at the same angular positions under different operating speeds. However, this does not imply that the function remains optimal at other speeds. Therefore, simulations at 100 r/min, 200 r/min, and 400 r/min are conducted to evaluate the cross-speed reuse performance of the same optimized TSF after the learning process is terminated, thereby verifying its capability to suppress torque ripple under the tested operating conditions.

4 Simulation results and analysis

An 8/6-pole SRM model is implemented in MATLAB/Simulink to evaluate the proposed strategy. The motor specifications are listed in Table 2. A lookup-table approach is used for nonlinear modeling: flux linkage and torque data are obtained using the RMxprt and Maxwell 2D modules in Ansys Electronics and imported into two-dimensional lookup-table blocks. The actual motor torque is determined from the torque data using the instantaneous current i and rotor position angle θ.

Table 2. SRM specifications.

Parameter	Value
Stator/rotor poles	8/6
Rated power (kW)	4
Rated speed (r/min)	1500
Stator outer/inner diameter (mm)	120/74.5
Rotor outer/inner diameter (mm)	74/30
Stack length (mm)	65

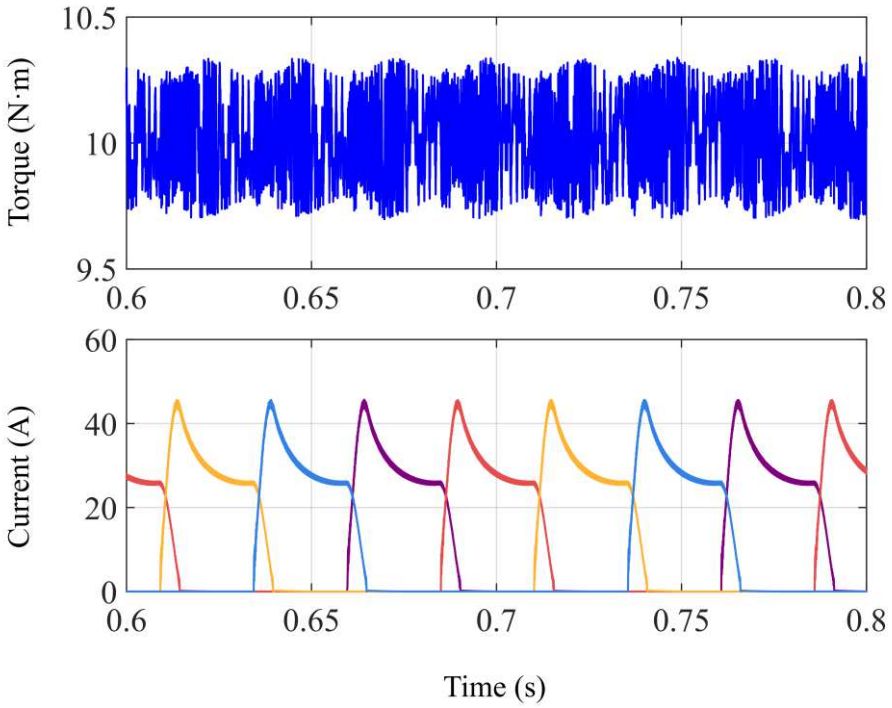
The torque ripple ratio is defined as[21]

$$K_r = \frac{T_{\max} - T_{\min}}{T_{av}} \times 100\% \tag{20}$$

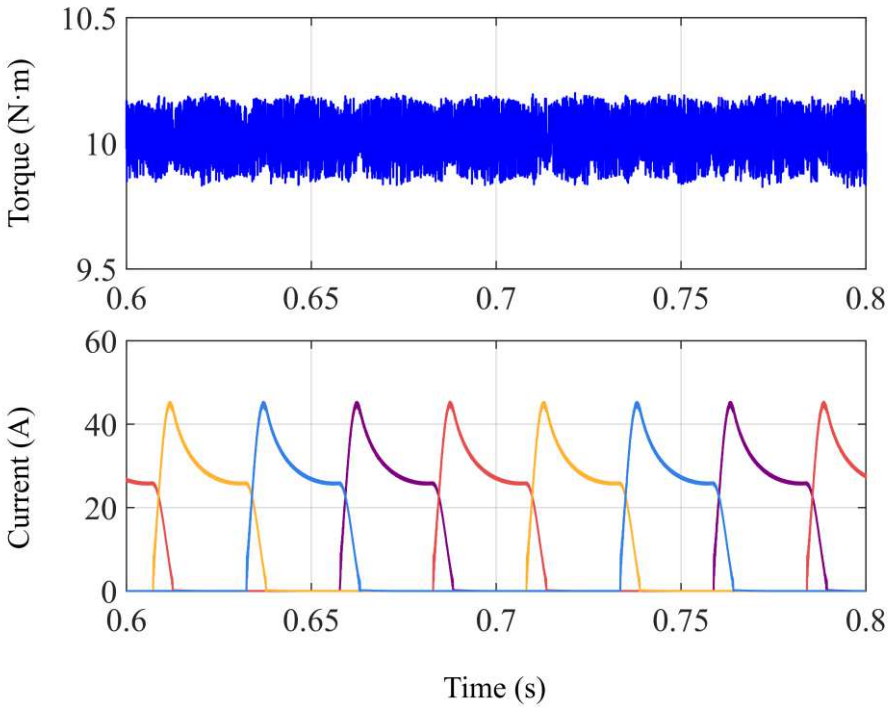
Where $T_{\max}$, $T_{\min}$, and T_{av} are the maximum instantaneous torque, minimum instantaneous torque, and average torque, respectively.

Conventional TSF control and the proposed control strategy are compared at a load torque of 10 $\mathrm{N \cdot m}$. Three representative steady-state speeds, 100, 200, and 400 r/min, are considered. The torque and phase current waveforms are examined to compare the performance of the two strategies.

Figure 8 compares the torque and phase current waveforms obtained with conventional TSF control and the proposed ILC-TSF strategy at 100 r/min. The corresponding torque ripple ratios are 6.50% and 3.92%, respectively.



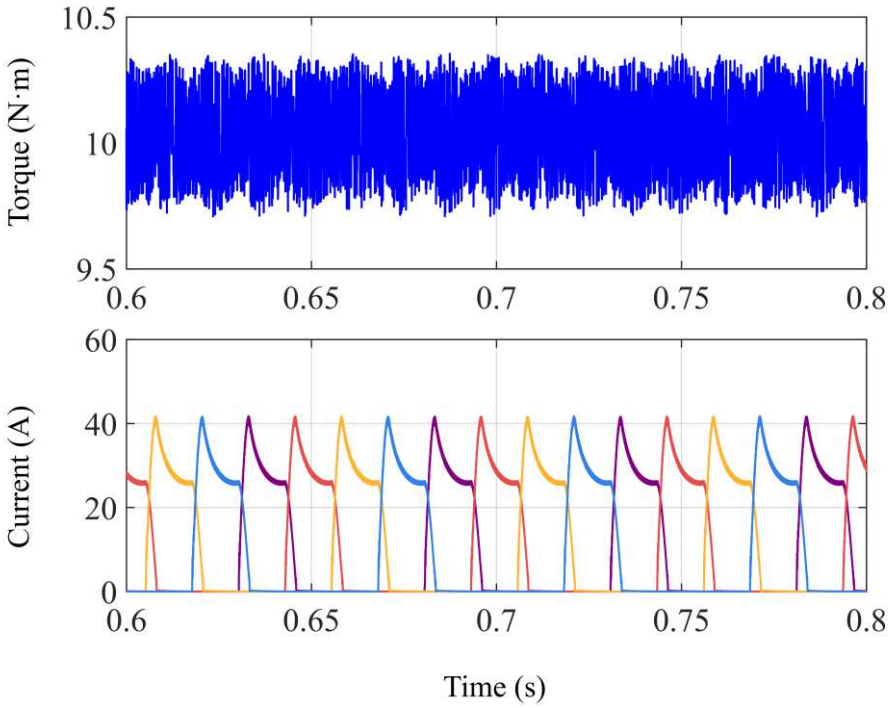
(a) Conventional TSF control at steady state



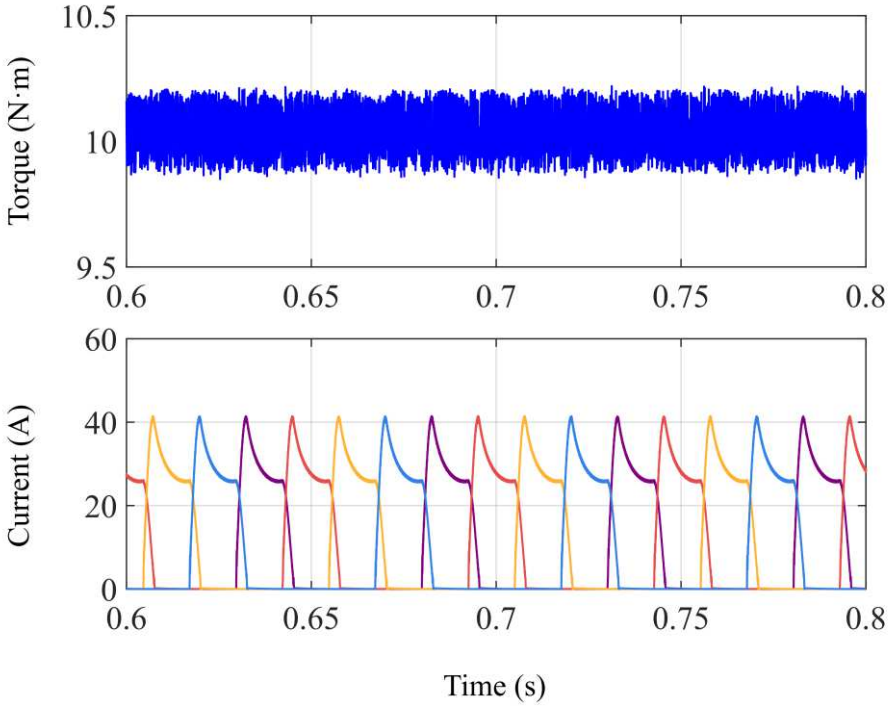
(b) ILC-TSF control at steady state

Fig. 8. Simulation results for the two control strategies at 100 r/min.

Figure 9 compares the torque and phase current waveforms at 200 r/min. Conventional TSF control produces a torque ripple ratio of 6.51%, whereas the proposed strategy reduces it to 3.98%.



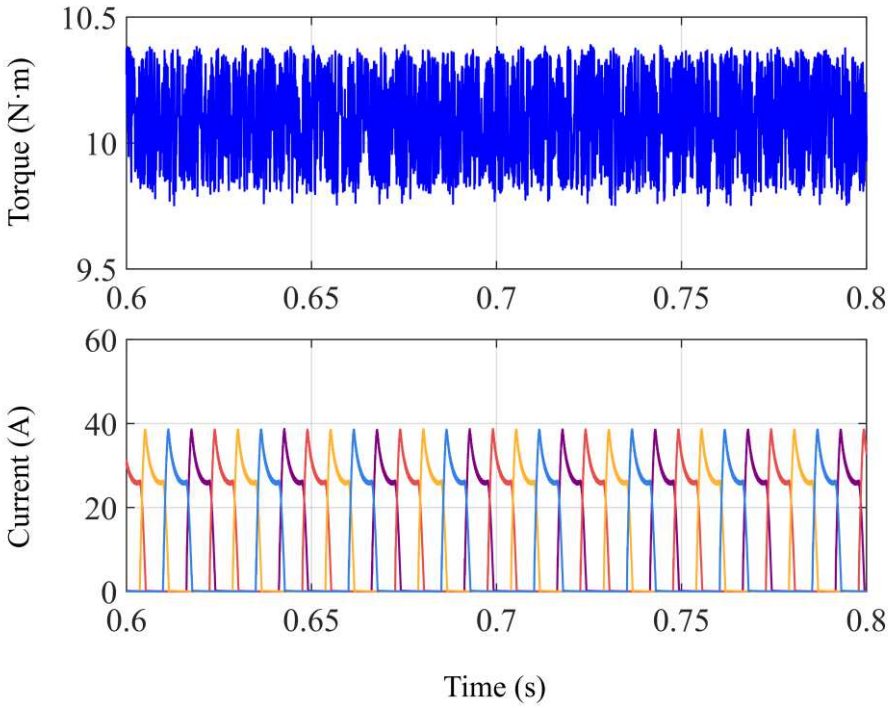
(a) Conventional TSF control at steady state



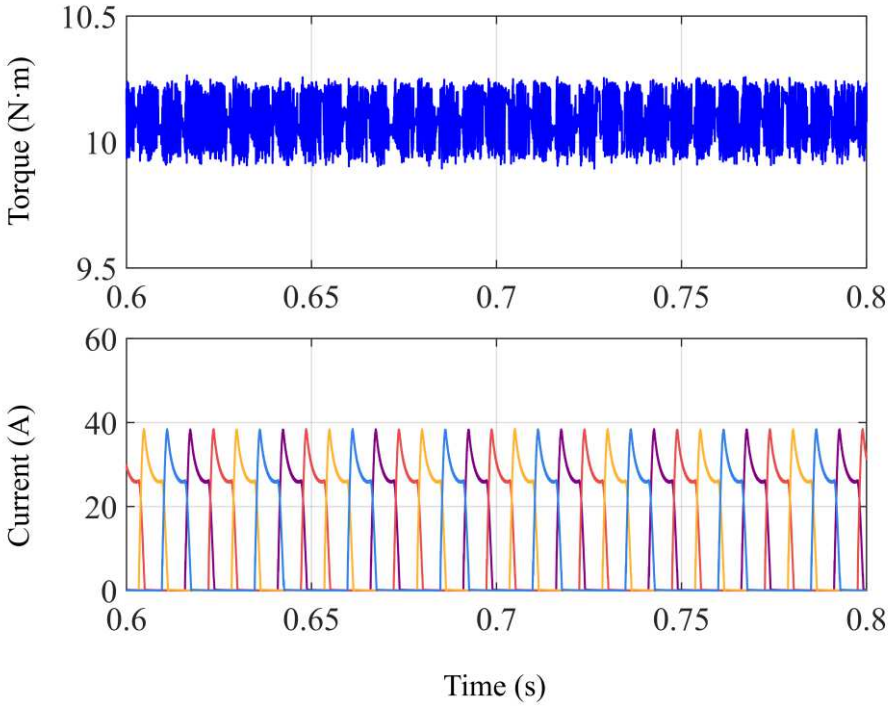
(b) ILC-TSF control at steady state

Fig. 9. Simulation results for the two control strategies at 200 r/min.

Figure 10 presents the torque and phase current waveforms at 400 r/min. The torque ripple ratios obtained with conventional TSF control and the proposed ILC-TSF strategy are 6.32% and 3.90%, respectively.



(a) Conventional TSF control at steady state



(b) ILC-TSF control at steady state

Fig. 10. Simulation results for the two control strategies at 400 r/min.

Table 3 summarizes the torque ripple ratios at the three speeds. Relative to conventional TSF control, the proposed strategy reduces the torque ripple ratio by 39.69%,38.86%, and 38.29% at 100 r/min, 200 r/min, and 400 r/min, respectively. These results demonstrate effective torque ripple suppression under the low-speed steady-state conditions considered.

Table 3. Comparison of torque ripple ratios at different speeds.

Method	Speed (r/min)	T_{max} (N·m)	T_{min} (N·m)	K_r (%)
TSF	100	10.34	9.690	6.50
TSF	200	10.36	9.709	6.51
TSF	400	10.38	9.748	6.32
ILC-TSF	100	10.21	9.818	3.92
ILC-TSF	200	10.23	9.832	3.98
ILC-TSF	400	10.27	9.880	3.90

5 Conclusions

An ILC-based TSF optimization strategy is proposed to reduce torque ripple in SRMs operating at low speed under steady-state conditions. The method iteratively corrects the TSF using periodic torque errors, improving agreement between the reference and actual torques and smoothing torque transfer during commutation. Compared with conventional TSF control, the proposed strategy reduces the simulated torque ripple ratio by 39.69%,38.86%, and 38.29% at 100, 200, and 400 r/min, respectively. These results demonstrate the effectiveness of the strategy for low-speed steady-state torque ripple suppression.

However, its performance at medium and high speeds requires further improvement. The present validation is limited to simulation, and experimental verification using a physical prototype remains necessary.

Future work will address three aspects. First, the ILC parameters and learning algorithm will be further optimized to improve torque ripple suppression at medium and high speeds and extend the applicable speed range. Second, a more comprehensive efficiency assessment will be developed, accounting for copper loss, iron loss, and other losses to evaluate the effect of the strategy on SRM efficiency. Third, prototype experiments will be conducted and compared with the simulation results to further assess the feasibility and effectiveness of the proposed method.

Data availability

All data generated or analysed during this study are included in this article.

References

1 Qiu, L. *et al.* Networked control strategy of dual linear switched reluctance motors based time delay tracking system. *ISA Transactions* **129**, 605–615 (2022). https://doi.org/10.1016/j.isatra.2021.12.034

2 Lan, Y. *et al.* Switched reluctance motors and drive systems for electric vehicle powertrains: State of the art analysis and future trends. *Energies* **14** (2021). https://doi.org/10.3390/en14082079

3 Sun, X., Wu, J., Lei, G., Guo, Y. & Zhu, J. Torque Ripple Reduction of SRM Drive Using Improved Direct Torque Control with Sliding Mode Controller and Observer. *IEEE Transactions on Industrial Electronics* **68**, 9334–9345 (2021). https://doi.org/10.1109/TIE.2020.3020026

4 Szabo, L. in *10th International Conference on Electrical Power Drive Systems, ICEPDS 2018, October 3, 2018 - October 6, 2018.* (Institute of Electrical and Electronics Engineers Inc.).

5 Tariq, I., Muzzammel, R., Alqasmi, U. & Raza, A. Artificial Neural Network-Based Control of Switched Reluctance Motor for Torque Ripple Reduction. *Mathematical Problems in Engineering* **2020** (2020). https://doi.org/10.1155/2020/9812715

6 Li, Z., Wang, S., Zhou, L. & Gan, C. Torque Ripple Suppression Method for Switched Reluctance Motor Based on Current Adaptive Torque Sharing Function. *IEEE Transactions on Transportation Electrification* **11**,

11216–11227 (2025). https://doi.org/10.1109/TTE.2025.3574077

7 Jing, B., Dang, X., Liu, Z. & Ji, J. Torque Ripple Suppression of Switched Reluctance Motor with Reference Torque Online Correction. *Machines* **11**, 179 (2023).

8 Ye, J., Bilgin, B. & Emadi, A. An Offline Torque Sharing Function for Torque Ripple Reduction in Switched Reluctance Motor Drives. *IEEE Transactions on Energy Conversion* **30**, 726–735 (2015). https://doi.org/10.1109/TEC.2014.2383991

9 Li, H., Bilgin, B. & Emadi, A. An Improved Torque Sharing Function for Torque Ripple Reduction in Switched Reluctance Machines. *IEEE Transactions on Power Electronics* **34**, 1635–1644 (2019). https://doi.org/10.1109/TPEL.2018.2835773

10 Fei, C., Yan, J., Wang, P. & Yan, Z. Torque Ripple Suppression of Switched Reluctance Motor Based on Modified Torque Sharing Function. *Diangong Jishu Xuebao/Transactions of China Electrotechnical Society* **33**, 394–400 (2018). https://doi.org/10.19595/j.cnki.1000-6753.tces.180593

11 Chen, X. & Peng, Y. Torque-ripple minimization for SRMs with segmental rotors and fully-picthed windings based on TSF by current compensation strategy. *Diangong Jishu Xuebao/Transactions of China Electrotechnical Society* **29**, 131–138 (2014).

12 Ai, W., Hu, L.-W., Li, X.-Y. & Li, X.-L. Active disturbance rejection based iterative learning control for torque ripple suppression in switched reluctance motor. *Kongzhi Lilun Yu Yingyong/Control Theory and Applications* **37**, 2098–2106 (2020). https://doi.org/10.7641/CTA.2020.91037

13 Lai, C., Zheng, Y., Labak, A. & Kar, N. C. in *21st International Conference on Electrical Machines, ICEM 2014, September 2, 2014 - September 5, 2014.* 796–802 (Institute of Electrical and Electronics Engineers Inc.).

14 Liu, D., Fan, Y., Liu, J., Wang, G. & Sun, D. Deadbeat Indirect Torque Control of Switched Reluctance Motors with Current Vector Decomposition. *Journal of Electrical Engineering and Technology* **19**, 4953–4968 (2024). https://doi.org/10.1007/s42835-024-01891-y

15 Mahalakshmi, G. & Kanthalakshmi, S. in *8th International Conference on Advanced Computing and Communication Systems, ICACCS 2022, March 25, 2022 - March 26, 2022.* 299–304 (Institute of Electrical and Electronics Engineers Inc.).

16 Ren, H. *et al.* Iterative Learning Compensation for Parameter Robustness Enhancement of Deadbeat Current Control in FMDRM Drives. *IEEE Transactions on Industrial Electronics* **72**, 11048–11058 (2025). https://doi.org/10.1109/TIE.2025.3557995

17 Xu, K., Meng, B., Wang, Z. & Huang, X. Robust PID-Type Iterative Learning Control for Nonlinear Square and Nonsquare Systems. *IEEE Transactions on Neural Networks and Learning Systems* **37**, 148–160 (2026). https://doi.org/10.1109/TNNLS.2025.3601656

18 Khattak, S., Hussain, I., Gomez-Aguilar, J. F. & Jan, R. Analysis of PD-type iterative learning control for discrete-time singular system. *Mathematical Methods in the Applied Sciences* **49**, 1315–1328 (2026). https://doi.org/10.1002/mma.7685

19 Cai, H. *et al.* Torque ripple reduction for switched reluctance motor with optimized PWM control strategy. *Energies* **11** (2018). https://doi.org/10.3390/en11113215

20 Xiao, Z., Zhang, G. & Huang, Y. in *32nd Chinese Control and Decision Conference, CCDC 2020, August 22, 2020 - August 24, 2020.* 189–192 (Institute of Electrical and Electronics Engineers Inc.).

21 Wu, J., Wang, H., Li, L., Yang, Y. & Guo, Z. Direct instantaneous torque control strategy for vehicle SRM based on improved convergence rate sliding mode control. *Scientific Reports* **15**, 27130 (2025). https://doi.org/10.1038/s41598-025-06550-4

Author contributions

Conceptualization was done by J.W. and S.L.; methodology was done by J.W.; software was done by S.L.; validation was done by J.W. and S.L.; formal analysis was done by Y.Y. and L.L.; investigation was done by Y.Y. and Z.W; resources was done by J.W.; data curation was done by J.W.; writing—original draft preparation was done by S.L. and J.W; writing—review and editing was done by J.W. All authors have read and agreed to the published version of the manuscript.

Funding

This research was funded by Henan Province University Science and Technology Innovation Team Support Program, grant number 24IRTSTHN029.

Competing interests

The authors declare no competing interests.

Additional information

Correspondence and requests for materials should be addressed to J.W.

Legends

Figure legends

Fig. 1. Structure of the 8/6-pole SRM.

Fig. 2. Schematic of the cosine TSF.

Fig. 3. Mechanism of torque ripple in TSF control.

Fig. 4. Block diagram of the ILC-TSF control system.

Fig. 5. Construction of the TSF update law.

Fig. 6. Torque ripple ratio versus learning gain. (a) Overall variation curve;(b) Enlarged view of the local region.

Fig. 7. Torque ripple ratio versus iteration number.

Fig. 8. Simulation results for the two control strategies at 100 r/min. (a) Conventional TSF control at steady state;(b) ILC-TSF control at steady state.

Fig. 9. Simulation results for the two control strategies at 200 r/min. (a) Conventional TSF control at steady state;(b) ILC-TSF control at steady state.

Fig. 10. Simulation results for the two control strategies at 400 r/min.(a) Conventional TSF control at steady state;(b) ILC-TSF control at steady state.

Table legends

Table 1. Torque ripple ratio for selected learning gains in the low-gain range.

Table 2. SRM specifications.

Table 3. Comparison of torque ripple ratios at different speeds.